INFLUENCE OF TRIBOLOGY OF CAGE MATERIAL ON BALL BEARING CAGE INSTABILITY

C. Servais, M. Duquenne, and J.-L. Bozet

Cryotribologie, Département de Chimie Appliquée, Université de Liège (ULg), Allée du 6 Août, B4000, Liège, Belgium,
Emails: c.servais@ulg.ac.be; marc.duquenne@ulg.ac.be; jlbozet@ulg.ac.be

ABSTRACT

By creating a solid lubricant thickness on both bearing races, a cage material of cryogenic ball bearing plays a significant role in the good dynamical behavior of the cage. This role is essential because of the lack of conventional lubricant into this kind of bearing.

In this paper, a method able to identify if a particular potential cage material can correctly fulfill its function is described. In other words, if it can lead to a stable movement of the cage. From the identification of fundamental tribological parameters governing the cage behavior, this method presents an example of ranking of such materials. This is based on pin-on-disk tests and on a numerical approach.

1. INTRODUCTION

Cryotechnic ball bearings of rocket engine turbopump work in liquid oxygen or liquid hydrogen. These fluids are seen as good cooling agents. They are able to drain the heat initiated by the friction between the balls and the races of the bearing. However, their low viscosity cannot produce a sufficient thickness. As a result, there is no separation between those parts. In order to solve this issue, a system was developed to provide a satisfying lubrication. The idea is to store the lubricant on the cage of the ball bearing. When ball and cage have repeated contacts, the lubricant, situated into each pocket of the separator, is taken away little by little and then settles on races (this is known as double transfer). This kind of lubrication is called solid lubrication.

Despite this method, frictional phenomena remain an issue for this kind of ball bearing. Indeed, repeated hits between the cage, rolling elements and races induce, under certain circumstances, an unstable movement of the separator. More precisely, this is the energy transfers obtained by friction between the cage and its environment that control the stable or unstable behavior of the cage. The instability phenomenon sharply increases internal transient loads that can lead to ball bearing failure [1].

2. CAGE INSTABILITY PREDICTION

From a general point of view, the comprehensive description of the cage movement necessitates a dynamical model with 6 degrees of freedom. Nevertheless, Kannel and Bupara [2], whose modeling is based on experimental facts, concluded that the cage trajectory can be studied in the ball bearing plane. This considerably facilitates the modeling of cage dynamics. Besides the possibility of using this dynamical model with a quasi-static model of the ball bearing, the Kannel and Bupara approach deals with two fundamental tribological parameters. Those one give a way to determine if the cage is stable or not.

2.1. Fundamental parameters

2.1.1. Restitution factor

The first parameter is the restitution factor (η). It is defined as the ratio of the circumferential speeds of the cage, after ($V^{\mathrm{f}}_{\mathrm{cage}}$) and before ($V^{\mathrm{i}}_{\mathrm{cage}}$) an impact with a ball, respectively (see figure 3). So one has

$$\eta = \frac{V^{\mathrm{f}}_{\mathrm{cage}}}{V^{\mathrm{i}}_{\mathrm{cage}}} \tag{1}$$

This coefficient depends on lubricating conditions found at the ball/race interface. A high value of η, close to one, reflects an insufficient lubrication. On the contrary, an improvement in the lubrication reduces the speed rendered by the balls to the cage. This leads to a lower restitution factor, tending to zero.

In dry operating conditions, with the eventual presence of a solid lubricant, η is function of the load applied to the ball bearing and the ball/race traction coefficient (C_T). By definition, this coefficient is the ratio of the tangential force (T) and the normal load (N) at the contact level:

$$C_T = \frac{T}{N} \tag{2}$$

This ratio must not be confused with the ball/race friction coefficient (f_{BT}), which is the quotient T/N but only in

'15th European Space Mechanisms & Tribology Symposium – ESMATS 2013'
Noordwijk, The Netherlands, 25–27 September 2013

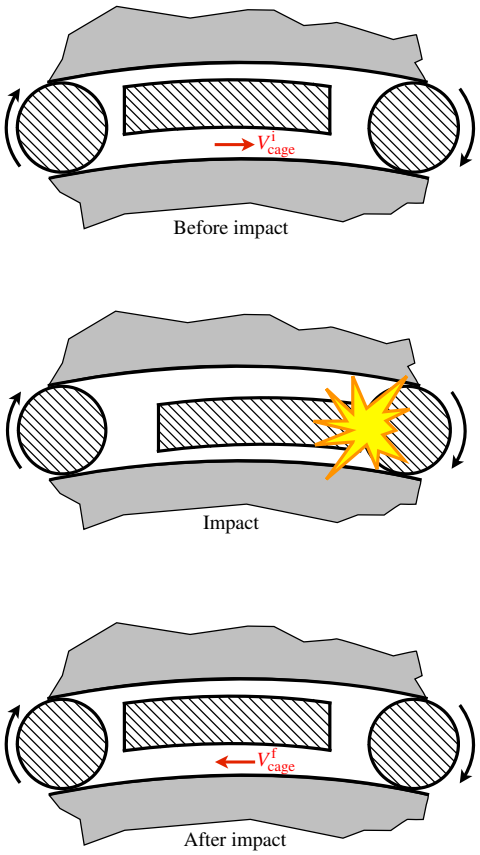

Figure 1. Ball/cage impact and circumferential speeds.

the case of pure sliding. By contrast, the traction coefficient (C_T) takes into account the relative rotation between ball and race.

2.1.2. Friction coefficient

The second parameter is the friction coefficient of the ball/cage contact (f_{BC}). During a shock, the difference of speed between the separator and a ball leads to a pure sliding.

2.2. Stability curve

An example of cage instability prediction, as a function of the ball/cage friction coefficient and the restitution factor, is given in Fig. 2. This stability curve was plotted for typical bearing geometry and operating conditions of cryogenic engine (DN parameter of 0.75 million, axial load of 300 daN). The area situated under the curve includes all points (η, f_{BC}) for which the separator is stable. By contrast, the cage is unstable for the points located above the curve.

Kannel and Bupara's modeling of the cage dynamics was thus included in an original quasi-static study of the ball

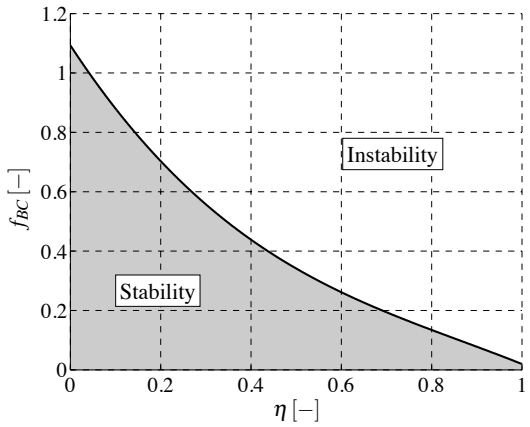

Figure 2. Stability curve example.

bearing [3]. This one leads to the ball bearing kinematics with great accuracy. Sec. 4.4 of this paper shows why this feature is essential to determine the ball/race traction coefficient (C_T).

3. PIN-ON-DISK TESTS IN CRYOGENIC ATMOSPHERE

Name	Composition
Meldin HTC 100	Polyimide + carbon fibers
Meldin 7211	Polyimide + graphite + PTFE
Armalon	PTFE + glass fibers
PEEK WG 101	Polyether ether ketone + additives (PTFE free)
PEEK 450 GL 30	Polyether ether ketone + glass fibers
PEEK450 CA 30	Polyether ether ketone + glass fibers + PTFE
Vespel SP 211	Polyimide + graphite + PTFE

Tableau 1. Potential cage materials which were tested.

Tests were performed using a pin-on-disk tribometer in order to quantify the cage/race or cage/ball friction coefficient for a range of potential cage materials. The tribometer works under cryogenic atmosphere, reproduces a slip speed from 1 to 5 m/s and applies a pin-on-disk normal load from 1 to 14 daN [4].

The pin is the potential cage material to be tested and the disk, which plays either the role of the balls or the

bearing races, is made of stainless steel (Chromex 40 or 440C). The potential cage materials are listed in Tab. 1. All the couples of materials were tested in both liquid and gaseous nitrogen, at a temperature of 77 K.

Tests were conducted on a wide range of slip speed (V) and contact pressure (p) for each potential cage material. Those parameters were adjustable independently on the tribometer. The pV products reached during tests are listed in Tab. 2.

Tribological test results are included in Tab. 3. The values presented in this table are the mean values of friction coefficients measured for the pV products described in Tab. 2.

p [MPa] \ V [m/s]	1	2	3	4	5
0,5	0,5	1	1,5	2	2,5
1	1	2	3	4	5
3	3	6	9	12	15

Tableau 2. List of pV products reached during tribological tests.

4. BALL/RACE CONTACT MODEL

4.1. Contact pressure

Since balls are loaded between both bearing rings, local deformations appear at ball/race contacts. The Hertz theory [5] allows to characterize: the surface shape for bodies pressed together, the contact pressure and the relationship between the normal load and the normal displacement within the contact.

According to the Hertz theory, the contact shape formed by two non conformal bodies is an ellipse with a semi-major axis a and a semi-minor axis b. The semi-major axis is in the transverse direction of the ring groove. The two parameters are only a function of the bodies geometry (not deformed) and of the normal load which tends to bring them closer. The pressure distribution is a semi-ellipsoid.

4.2. Contact slip speed field

Contacts between balls and bearing rings are submitted to slip phenomena that come out two sources. They are described below by taking the example of the relative ball/inner race movement (the explanation is the same for the relative ball/outer race movement).

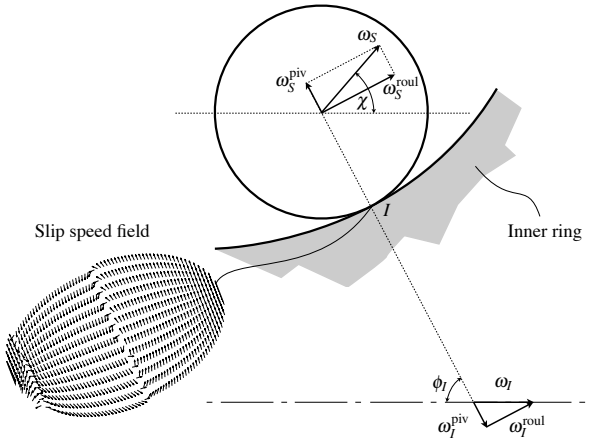

Figure 3. Ball kinematics for a ball/inner race contact.

– The first source is the rolling movement of the ball relative to the ring. One considers the rotational speeds ω_S^{roul} and ω_I^{roul} (figure 3), respectively the vector components of the ball spin (ω_S) and the rotational speed of the inner ring (ω_I) within the contact plane. The elongated shape of the Hertzian ellipse, due to the transverse curvature of the ring groove, leads to a variation of the slip speed along the major axis of the ellipse. This kind of rolling friction due to close conformity was identified by Heathcote [5].

– The second source of slip comes from the pivoting movement of the ball relative to the ring. Rotational speeds involved are ω_S^{piv} and ω_I^{piv}, respectively the vector components of the ball spin (ω_S) and the rotational speed of the inner ring (ω_I) in the direction that is perpendicular to the contact plane.

Rolling and pivoting components result in a slip speed field for which an example is depicted in Fig. 3.

The slip speed field can be described by using the *creep ratio*. This is a dimensionless parameter defined as

$$\xi_I(y) = \frac{V_B(y) - V_I(y)}{V_I^{roul}} \tag{3}$$

$$= \underbrace{\left.\frac{V_B(y) - V_I(y)}{V_I^{roul}}\right|_{roul}}_{\substack{\text{rolling} \\ \text{component}}} + \underbrace{\left.\frac{V_B(y) - V_I(y)}{V_I^{roul}}\right|_{piv}}_{\substack{\text{pivoting} \\ \text{component}}} \tag{4}$$

$$= \xi_I^{roul}(y) + \xi_I^{piv}(y) \tag{5}$$

where V_B is the peripheral speed of the ball, V_I is the peripheral speed of the inner ring and V_I^{roul} is the incoming speed of points from ball and inner ring within the contact zone.

	Gaseous nitrogen Chromex 40 disk	Gaseous nitrogen 440C disk	Liquid nitrogen, Chromex 40 disk	Liquid nitrogen 440C disk
Meldin HTC 100	×	×	0,22	0,32
Meldin 7211	0,1	0,13	0,18	0,2
Armalon	0,09	0,07	0,05	0,08
PEEK WG 101	0,1	0,17	0,15	0,14
PEEK 450 GL 30	0,29	0,16	0,39	0,27
PEEK 450 CA 30	0,11	0,17	0,12	0,13
Vespel SP 211	0,12	0,13	0,14	0,11

Tableau 3. Friction coefficients measured by the pin-on-disk tribometer as a function of the test conditions.

4.3. Tangential tractions

The slip speed field described above implies a local tangential displacement within the contact due to elastic compliance. It is possible to calculate those deformations and determine the tangential tractions. Some assumptions have therefore to be taken into consideration.

4.3.1. Assumptions

In this subsection, we list the assumptions required.

- Hertzian pressure (p) is completely independent of the tangential traction ($\bar{\tau}$) within the contact.
- The ball bearing works in a steady state.
- Materials remain in the elastic domain, with linear strain.
- The solid lubricant on races is a softer material than the stainless steel of balls and rings.
- Slip speeds parallel to the major-axis a of the contact are neglected. This is licit because of the high ratio b/a [5].
- The contact surface can be divided into a series of strips (width of Δy each), which are parallel to the minor-axis b and independent of each other. This assumption, made for the first time by Haines and Ollerton [6] and called *strip theory*, is valid if the tangential traction does not vary a lot along the semi-major axis of the ellipse. This is especially the case for elongated ellipses [5, 7].
- The ball/track friction coefficient (f_{BT}) is a constant, no matter the slip speed or the pressure involved.

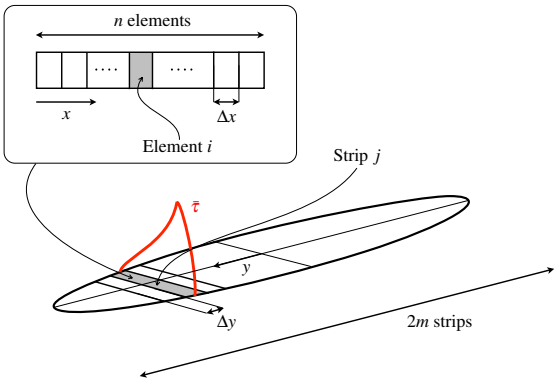

Figure 4. Contact scheme, illustration of the strip theory.

4.3.2. No slip assumption

When slip occurs within the contact, the ball/track friction coefficient is defined as

$$f_{BT} = \frac{\bar{\tau}}{p} \tag{6}$$

Firstly, one considers that f_{BT} tends to infinity, that is to say that no slip takes place within the contact. Then, one can calculate the strain in each strip. For a given strip of ordinate y_j, one has (Fig. 5)

$$u_I(x) + u_S(x) = \xi_I(y_j)\, x \tag{7}$$

since time is related to the abscissa x in a steady state

$$x = V_I^{\text{roul}} t \tag{8}$$

One has to note that the displacements involved here are relative to the displacement in $x = 0$.

By discretizing the strips into n parts having each a width of Δx (Fig. 4), it is possible to find the stiffness matrices $\mathbf{K}_I$ and $\mathbf{K}_S$ that link the n nodes. Thus

$$\begin{cases} \mathbf{K}_I \mathbf{q}_I = \mathbf{g} \\ \mathbf{K}_S \mathbf{q}_S = \mathbf{g} \end{cases} \Longleftrightarrow \begin{cases} \mathbf{q}_I = \mathbf{K}_I^{-1} \mathbf{g} \\ \mathbf{q}_S = \mathbf{K}_S^{-1} \mathbf{g} \end{cases} \tag{9}$$

with

$$\begin{aligned} \mathbf{q}_I &= \{u_I(x_1) \dots u_I(x_n)\}^T \\ \mathbf{q}_S &= \{u_S(x_1) \dots u_S(x_n)\}^T \\ \mathbf{g} &= \{\bar{\tau}(x_1) \dots \bar{\tau}(x_n)\}^T \Delta x \end{aligned} \tag{10}$$

The relationships (9) coupled to (7) join the tangential tractions distribution to the speeds within the contact. One has

$$\mathbf{g} = \left(\mathbf{K}_I^{-1} + \mathbf{K}_S^{-1}\right)^{-1} \xi_I \mathbf{x} \tag{11}$$

with $\mathbf{x} = \{x_1 \dots x_n\}^T$.

The calculation of the stiffness matrices is realized by means of the method described in [5], in the case of a half-space submitted to a line loading. In addition to this, a method developed by Dareing [8] (firstly elaborated to study cylinder on cylinder contact) linking metallic substrates (ball and rings) to the transfer film was used.

4.3.3. Presence of slip

At some points within the ball/track contact, tangential tractions calculated using (11) are superior to the limit imposed by Coulomb (6). Thus, by means of an iterative process, one has to put those particular tangential tractions

$$\bar{\tau} > f_{BT}\, p \tag{12}$$

to an admissible level

$$\bar{\tau} = f_{BT}\, p \tag{13}$$

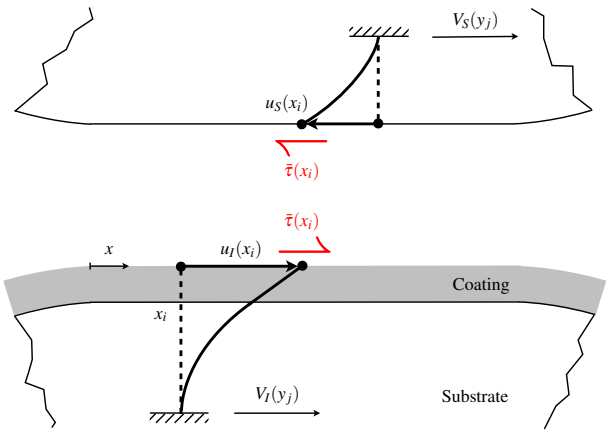

Figure 5. Speeds and displacements within one of the contact strips.

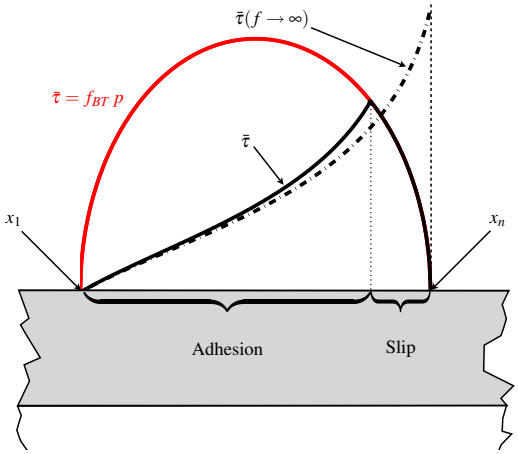

Figure 6. Arbitrary strip chosen within the contact. Tangential tractions without slip (dashed black line), with slip (solid line) and physical limit imposed by Coulomb.

Fig. 6 gathers all the tangential tractions mentioned above, for an arbitrary strip chosen within the contact. Without coating, the black solid line tends to Carter's solution, which is the traction distribution between two isotropic cylinders [9].

The main originality of the presented model is to take into account the complex kinematics of the ball bearing and to sum the contribution of each strip in order to obtain the complete tangential traction distribution within the coated Hertzian contacts of the bearing.

4.4. Traction coefficient

When a ball/cage impact occurs, the cage induces a slight variation ΔV in the ball speed. By taking the example of the ball/inner race contact again, this variation leads to a new contribution $\delta\xi_I$ to the creep ratio

$$\xi_I(y) = \xi_I^{\text{roul}}(y) + \xi_I^{\text{piv}}(y) + \underbrace{\delta\xi_I}_{\frac{\Delta V}{V_I^{\text{roul}}}} \tag{14}$$

The sign of $\delta\xi_I$ changes depending on the location of the shock (in front of the ball or behind it).

The fluctuation of the ball speed causes a variation in the traction load T_I, which is the resultant force of traction distribution

$$T_I = \sum_{j=1}^{2m} \sum_{i=1}^{n(y_j)} \bar{\tau}(x_i, y_j) \Delta x(y_j)\, \Delta y \tag{15}$$

The presented contact model permits to calculate T_I as a function of the increment $\delta\xi_I$, and thus to quantify the traction coefficient C_T.

Examples of traction coefficient curve are presented in Fig. 7 for a typical ball/inner race contact. The curves

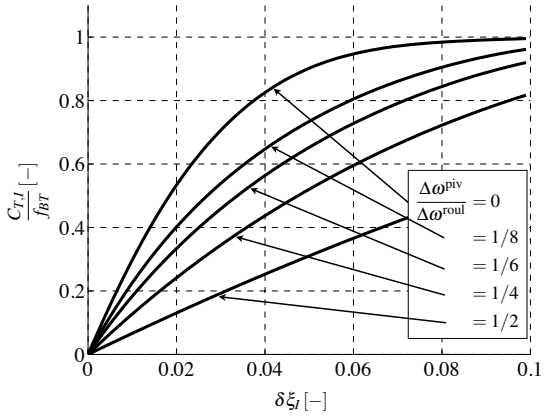

Figure 7. Example of traction coefficient curves for a ball/inner race contact and for several pivoting to rolling ratios.

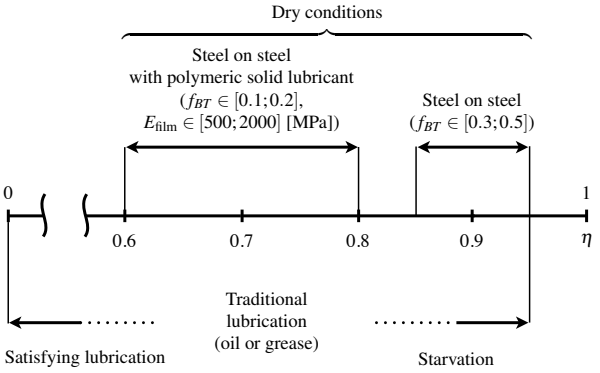

Figure 8. Orders of magnitude of the restitution factor η.

are plotted for several pivoting to rolling ratios, defined as (Fig. 3)

$$\frac{\Delta\omega^{\text{piv}}}{\Delta\omega^{\text{roul}}} = \frac{\omega_S^{\text{piv}} + \omega_I^{\text{piv}}}{\omega_S^{\text{roul}} - \omega_I^{\text{roul}}} \tag{16}$$

Those curves exhibit the importance of the pivoting component on the traction coefficient $C_{T,I}$. The use of the contact model is thus meaningful only if ball kinematics is known with accuracy, which is possible by using the quasi-static method [3].

The traction coefficient curve is function of:

- the friction coefficient of the ball/race contact that depends on the environment in which the ball bearing runs;
- the Young modulus E_{film} of the solid lubricant;
- the solid lubricant thickness h.

This is the slope α_I at the origin ($\delta\xi_I = 0$) which is particularly interesting from the point of view of the cage stability (see next section). This slope decreases while the friction coefficient f_{BT} and the ratio E_{film}/h increase.

4.5. Restitution factor calculation

Kannel and Bupara clearly showed [2] that the restitution factor (η) is a function of both slopes α_I and α_E of traction coefficient curves at the origin, respectively for inner and outer race contacts. One has

$$\eta = \exp\left(\frac{-\pi}{\sqrt{8\dfrac{C_\mu^2}{M_C k_{BC}} - 1}}\right) \tag{17}$$

where M_C is the cage mass, k_{BC} is the ball/cage contact stiffness and where

$$C_\mu = \frac{\alpha_I}{V_I^{\text{roul}}} N_I + \frac{\alpha_E}{V_E^{\text{roul}}} N_E \tag{18}$$

This relationship (17) establishes that, while the restitution factor increases, the slopes α_I and α_E decrease at the same time.

Fig. 8 gives orders of magnitude of restitution factor for different ball/race contact configurations. Values taken by the restitution factor in "dry" conditions were calculated using the contact model. The conclusions relative to the "traditional lubrication" come from [2].

5. APPLICATION

What one can conclude from Fig. 2 is that the friction coefficient has to be low and that the material tested also has to provide a good solid lubrication by means of the double transfer process, in order to reduce the restitution factor (Eqs. (17) and (18)).

Tests realized on the cryotribometer enable one to go further in the analysis. Indeed, knowing the ball/cage friction coefficient (f_{BC}) of all the materials implies that one can determine the threshold value of the restitution factor beyond which the separator becomes unstable. In other words, it is possible to directly see from the stability curve which lubricating conditions must be fulfilled. This is done by simply transposing the friction coefficients measured with pin-on-disk tests (see Tab. 3) on the stability curve of Fig. 2 and checking the value of the restitution factor.

Results are presented in Fig. 9, 10, 11 and 12. Those ones contain the tribological results for the two kinds of selected steels (Chromex 40 and 440 C).

The most appropriate material seems to be Armalon, according to these four graphs. Armalon has in fact the lowest ball/cage friction coefficient. Thus Armalon, used as cage material, does not require excessively good lubrication conditions ($\eta \approx 0.9$) as depicted in Fig. 8. Nevertheless, this result has to be moderated. Indeed, it was shown [10], for the particular situation of Armalon, that the ball/cage friction coefficient can greatly change within a cryotechnic ball bearing, as well as the roughness of the races. Because of the wear of cage pockets, Armalon glass fiber finally gets in contact with balls instead of Armalon PTFE and then settles on bearing races. These hard particles tend to completely use the lubricant layer made of PTFE, previously formed on bearing races.

On the other hand, using PEEK 450 GL 30 or Meldin HTC 100 as cage materials necessitate a fairly low restitution factor ($\eta < 0.6$). This threshold value is too low to be reached using solid lubrication. Consequently, they are inapt in this cryogenic atmosphere.

The four others materials tested (Meldin 7211, PEEK WG 101, PEEK CA 30 et Vespel SP 211) remain potential candidates. Their capacity to transfer from cage to races has yet to be established.

6. CONCLUSION

A way to evaluate cage material candidates, based on a recognized dynamical study of the cage, was developed in this paper. Especially, a new computational method leading to the restitution factor was proposed. From accurate values of ball/cage friction coefficient, measured by a cryogenic pin-on-disk tribometer, it was possible to classify a set of potential cage materials in order to fulfill the requirement.

The method described in the paper was applied, as an example, to a cryotechnic ball bearing of turbopump.

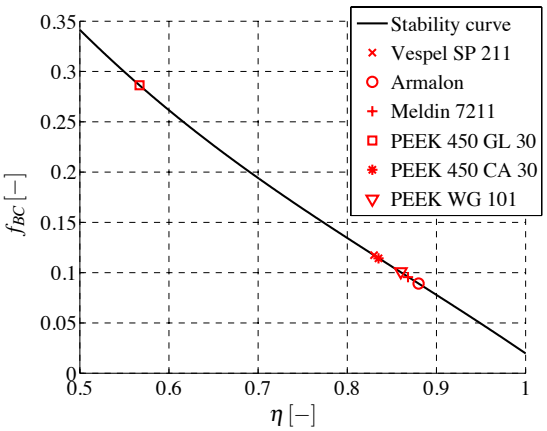

Figure 9. Stability curve: comparison of cage materials with a Chromex 40 disk, under gaseous nitrogen.

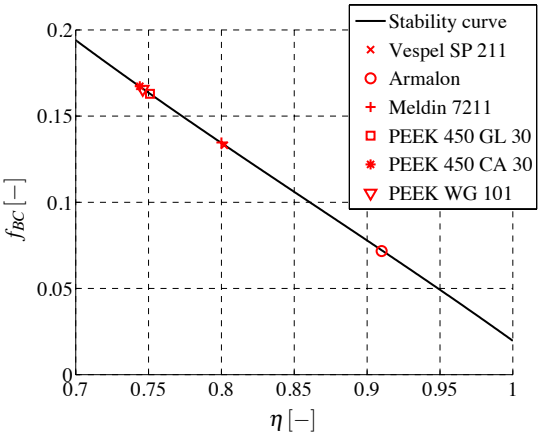

Figure 10. Stability curve: comparison of cage materials with a 440C disk, under gaseous nitrogen.

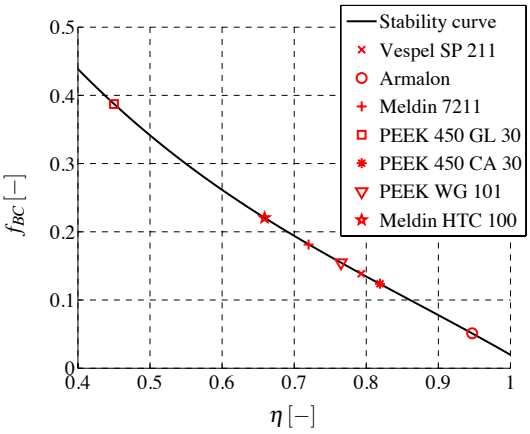

Figure 11. Stability curve: comparison of cage materials with a Chromex 40 disk, under liquid nitrogen.

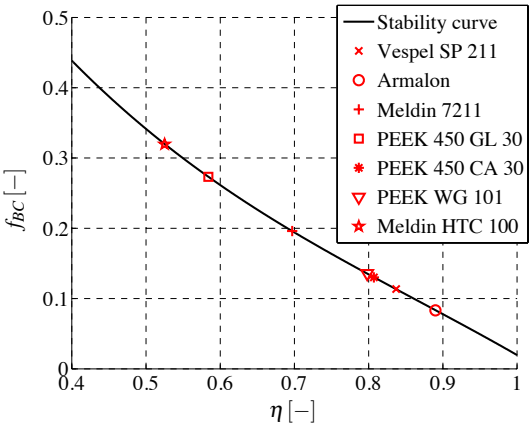

Figure 12. Stability curve: comparison of cage materials with a 440C disk, under liquid nitrogen.

Nevertheless, the method can be used in other frameworks, necessitating ball bearings working in dry conditions (satellites, high temperature operations,...).

The approach leading to the restitution factor necessitates some information about surface tribological properties of ball bearing rings, such as: ball/track friction coefficient, ability of cage material to form a solid lubricant layer on races, Young modulus and thickness of this layer. Thus, it appears that the present study has to be extended in order to evaluate those data (tribological tests, nanoindentation,...).

ACKNOWLEDGMENTS

Pin-on-disk test results were obtained in the FP7/ISP-1 (In Space Propulsion) project framework. The authors thank the concerned European authorities.

REFERENCES

[1] J. W. Kannel and D. K. Snediker. The hidden cause of bearing failure. *Machine Design*, pages 78–82, 1977.

[2] J. W. Kannel and S. S. Bupara. A simplified model of cage motion in angular contact bearings operating in the EHD lubrication regime. *Journal of Lubrication Technology*, vol. 100(3), juillet 1978.

[3] J.-L. Bozet. *Nouvelle approche du calcul des roulements à billes non lubrifiés*. PhD thesis, Université de Liège (ULg), mai 1996.

[4] J.-L. Bozet and R. Gras. Tribological behaviour of fluorinated resins and polyimide resins sliding over a metallic surface in liquid nitrogen. In W. R. Burke, editor, *Fifth European Space Mechanisms and Tribology Symposium*, pages 29–33. European Space Agency, 1992.

[5] K. L. Johnson. *Contact mechanics*. Cambridge University Press, 1985.

[6] D. J. Haines and E. Ollerton. Contact stress distributions on elliptical contact surfaces subjected to radial and tangential forces. In *Proceedings, Institution of Mechanical Engineers*, volume 177, pages 95–114, 1963.

[7] Joost Kalker. A strip theory for rolling with slip and spin. In *Koninklijke Nederlandse Akademie van Wetenschappen*, pages 10–62, 1967.

[8] D. W Dareing. Traction coefficients for coated bearing races lubricated with teflon transfer films. *Journal of Tribology*, Vol. 113, 1991.

[9] F. W. Carter. On the action of a locomotive driving wheel. In *Proceedings Containing Papers of a Mathematical and Physical Character*, volume 112 of *Series A*, pages 151–157. Royal Society of London, 1926.

[10] David E. Brewe, Herbert W. Scibbe, and William J. Anderson. Film-transfer studies of seven ball-bearing retainer materials in 33 K hydrogen gas at 0.8 million DN value. Nasa technical note, Lewis Research Center, Cleveland, Ohio, novembre 1966.

[11] A. B. Jones. The life of high-speed ball bearings. *Transactions of the ASME*, 74:695–703, juillet 1952.

[12] Pradeep K. Gupta. *Advanced dynamics of rolling elements*. Springer-Verlag, 1984.